The Astrophysical Journal, 749:128 (12pp), 2012 April 20 doi:10.1088/0004-637X/749/2/128

THE ROLE OF THERMOHALINE MIXING IN INTERMEDIATE- AND LOW-METALLICITY GLOBULAR CLUSTERS

George C. Angelou[1], Richard J. Stancliffe[1,2], Ross P. Church[1,3], John C. Lattanzio[1], and Graeme H. Smith[4]
[1] Monash Centre for Astrophysics, School of Mathematical Sciences, Monash University, Melbourne, VIC 3800, Australia; George.Angelou@monash.edu
[2] Research School of Astronomy & Astrophysics, Mt. Stromlo Observatory, Canberra, ACT 2611, Australia
[3] Department of Astronomy and Theoretical Physics, Lund Observatory, Box 43, SE-221 00 Lund, Sweden
[4] Department of Astronomy and Astrophysics, University of California Observatories/Lick Observatory, UC Santa Cruz, 1156 High Street, Santa Cruz, CA 95064, USA
Received 2011 August 30; accepted 2012 February 12; published 2012 March 30

ABSTRACT

It is now widely accepted that globular cluster red giant branch (RGB) stars owe their strange abundance patterns to a combination of pollution from progenitor stars and in situ extra mixing. In this hybrid theory a first generation of stars imprints abundance patterns into the gas from which a second generation forms. The hybrid theory suggests that extra mixing is operating in both populations and we use the variation of [C/Fe] with luminosity to examine how efficient this mixing is. We investigate the observed RGBs of M3, M13, M92, M15, and NGC 5466 as a means to test a theory of thermohaline mixing. The second parameter pair M3 and M13 are of intermediate metallicity and our models are able to account for the evolution of carbon along the RGB in both clusters, although in order to fit the most carbon-depleted main-sequence stars in M13 we require a model whose initial [C/Fe] abundance leads to a carbon abundance lower than is observed. Furthermore, our results suggest that stars in M13 formed with some primary nitrogen (higher C+N+O than stars in M3). In the metal-poor regime only NGC 5466 can be tentatively explained by thermohaline mixing operating in multiple populations. We find thermohaline mixing unable to model the depletion of [C/Fe] with magnitude in M92 and M15. It appears as if extra mixing is occurring before the luminosity function bump in these clusters. To reconcile the data with the models would require first dredge-up to be deeper than found in extant models.

Key words: globular clusters: individual (M3, M13, M15, M92, NGC 5466) – stars: abundances – stars: evolution – stars: Population II

Online-only material: color figures

1. INTRODUCTION

It is clear from the annals of stellar astrophysics that low-mass stars undergo mixing as they ascend the red giant branch (RGB hereafter; for example, see Charbonnel & Do Nascimento 1998). This is contrary to canonical models of red giants that incorporate convection as the only form of internal mass transport. Such models predict just one event capable of changing surface abundances of light elements on the first ascent of the RGB, namely the so-called first dredge-up (FDU; e.g., Iben 1967). However, a variety of observations indicate that some form of non-convective mixing (which is often termed "extra mixing" in the literature) progressively transports CN-processed material to the surface along the upper RGB while reducing the ^{12}C abundance. The effects of extra mixing are observed in field stars (Spite et al. 2005, 2006; Gratton et al. 2000; Charbonnel et al. 1998; Sneden et al. 1986) and globular cluster (GC) stars (Shetrone 2003; Recio-Blanco & de Laverny 2007) with increasing efficiency seen at lower metallicities. The mixing occurs internally as the star ascends the giant branch therefore variations in abundance manifest themselves as a function of luminosity. This is most clearly seen in carbon (Smith & Martell 2003) and lithium (Lind et al. 2009; Mucciarelli et al. 2011).

During the RGB phase of evolution the star possesses a degenerate hydrogen-exhausted core. A thin hydrogen burning shell progresses outward through the star contributing processed material to the inert core. A convective envelope which transports material to the stellar surface is separated from the shell by a radiative region. Extra mixing requires some mechanism to transport material across this radiative zone to the top of the hydrogen shell where it encounters temperatures where burning can occur. Processed material is cycled back to the convective envelope accounting for the observed compositions. Identifying the exact physics that induces this mixing has been debated at length; it has proven to be a challenging task for stellar astrophysics.

Phenomenological models of extra mixing can match the general abundance trends associated with further dredge-up of CN-processed material (Palmerini et al. 2011a, 2011b; Denissenkov & VandenBerg 2003; Wasserburg et al. 1995). Many physically based mechanisms have also been explored as potential candidates: rotational mixing (Sweigart & Mengel 1979; Chanamé et al. 2005; Palacios et al. 2006), magnetic fields (Palmerini et al. 2009; Nordhaus et al. 2008; Busso et al. 2007; Hubbard & Dearborn 1980), internal gravity waves (Denissenkov & Tout 2000), and more recently thermohaline mixing (Eggleton et al. 2006, 2008; Charbonnel & Zahn 2007a) and the combination of thermohaline mixing and magnetic fields (Denissenkov et al. 2009). Like any new paradigm, thermohaline mixing has stimulated a wealth of subsequent work (see Stancliffe 2010; Cantiello & Langer 2010; Charbonnel & Lagarde 2010; Angelou et al. 2011). The mechanism is initially driven by instabilities brought about from local inversions in the mean molecular weight. These inversions arise through the burning of ^{3}He. The reaction ^{3}He(^{3}He, $2p$)^{4}He produces more particles than it consumes. If this reaction can occur in a homogenized region, such as is the case when the hydrogen

burning shell advances through the composition discontinuity left by FDU, then its effect on the molecular weight profile can dominate (for a detailed explanation of the mixing process see Angelou et al. 2011). Understanding and modeling this mechanism is an area of active research at present (Wachlin et al. 2011; Traxler et al. 2011; Denissenkov & Merryfield 2011; Charbonnel & Zahn 2007b).

Charbonnel & Zahn (2007a) have shown that the mechanism can match the RGB abundances of field stars, with a dependence on metallicity which was also demonstrated by Eggleton et al. (2008). The next logical step was to test the mechanism against abundance measurements in GCs as Angelou et al. (2011) did with stars in M3. M3 was chosen as a test case because it is considered a typical GC. A metallicity of [Fe/H] $= -1.4$ (Sneden et al. 2004; Cohen & Meléndez 2005) means that it falls near the mode in the metallicity distribution of halo GCs. It is well studied and exhibits significant [C/Fe] depletion (Suntzeff 1981; Norris & Smith 1984; Smith et al. 1996; Smith 2002; Smith & Martell 2003; Martell et al. 2008b) as well as reduction in $^{12}C/^{13}C$ (Pilachowski et al. 2003; Pavlenko et al. 2003) along the RGB. Here we extend this work and compare M3 to its second parameter partner M13, thus testing the mechanism in another cluster of similar metallicity. We also turn to the more extreme end of the GC metallicity distribution by investigating the clusters M92, M15, and NGC 5466 (all with [Fe/H] ≈ -2.2). This sample allows us to investigate the mechanism in multiple clusters at a range of metallicities. The exercise is somewhat complicated by the fact that GCs possess multiple stellar populations.

Historically, GCs have been utilized as test beds for stellar theory. Some of the earliest published studies of GCs (Arp et al. 1952; Arp 1955; Sandage 1953) coincided with the first stellar evolution calculations (Oke & Schwarzschild 1952; Iben & Ehrman 1962). The initial mass spread of the stars and their presumed coeval nature contributed to the color–magnitude diagram's usefulness as a diagnostic tool for the developing theory (Sandage 1954; Johnson & Sandage 1955; Iben & Faulkner 1968). During this time GCs were considered to be simple stellar populations; that is, the stars in any given cluster were assumed to be of the same age and composition. Hence, the cluster color–magnitude diagram was an outcome of variations in stellar mass. The first study to challenge the simple stellar population hypothesis was that of Popper (1947). He measured CN band strength in the stars of M3 and M13 and found a CN-strong star among many CN weak stars. The importance of Popper's finding was highlighted by Osborn (1971) who found CN-strong stars in M5 and M10. These were the first clues that GCs possess heterogeneous C and N abundances.

The heterogeneity of stars within GCs extends beyond carbon and nitrogen. Along the RGB, as well as on the main sequence, O, Na, Mg, and Al can display star-to-star variations (e.g., Gratton et al. 2004 and Kraft 1994, and references therein). It is now commonly argued that a previous generation of stars polluted the medium from which a distinct second population formed. The first generation imprinted the abundance patterns from the various stellar burning sites, whether they were asymptotic giant branch stars (Fenner et al. 2004), super asymptotic giant branch stars (Ventura & D'Antona 2011), massive binaries (de Mink et al. 2009), or massive rotating stars (Brown & Wallerstein 1993; Smith 2006; Decressin et al. 2007; Charbonnel 2010). This scenario is consistent with the presence of C–N–O–Na abundance dispersions on the main sequences of GCs.

The formation of a second generation of stars from gas that is rich in CN-processed material provides a paradigm that explains the observations of dichotomous CN band strengths in GC stars. The CN band strength is a useful indicator of the nitrogen content of GC RGB star atmospheres. New stars that form from the polluted gas are inherently enriched in nitrogen as well as ^{4}He compared to the primordial generation (Norris et al. 1981). The fact that the dichotomy in the CN band strength has been detected below the bump in the luminosity function (LF bump), albeit for clusters that are of intermediate to high metallicity, provides strong evidence for the pollution scenario (Hesser & Bell 1980; Briley et al. 1991; Suntzeff & Smith 1991; Buonanno et al. 1994; Cannon et al. 1998; Cohen 1999; Briley & Cohen 2001; Pancino et al. 2010).

The CN bands can be used as population tracers in all but the most metal-poor clusters where [Fe/H] < -2 (e.g., Shetrone et al. 2010; Smolinski et al. 2011), since the CN bands are weak at low metallicity (Cohen et al. 2005). In such cases, the existence of multiple populations can be inferred through other means. Sneden et al. (1997, 2000) have shown that in metal-poor clusters [Na/Fe] varies by over 1 dex and this variation is not correlated with RGB evolution. The temperatures required for processing of Na are beyond those reached by thermohaline mixing on the RGB. We therefore expect a normal (primordial) and enriched population given the large spread. This is a strong indication that multiple populations do exist in these clusters.

Evidence of this multiple population scenario is not limited to the observations of CN band strength or variations in [Na/Fe]. It is discussed at length by Catelan et al. (2002), Anderson et al. (2009), and Piotto (2009, see references therein) for the main sequence and subgiant branch. Techniques such as isochrone fitting require distinct ^{4}He abundances in these populations to explain color–magnitude diagrams. Examples of such clusters include: Omega Centauri (Piotto et al. 2005; Lee et al. 2005; Sollima et al. 2007), NGC 2808 (D'Antona et al. 2005; Lee et al. 2005; Piotto et al. 2007), and 47 Tucanae (Anderson et al. 2009). We also note that calculations by D'Antona & Caloi (2008) show that the horizontal branches of various clusters can be best reproduced with the presence of two populations, one of which has elevated ^{4}He abundances, which is a prediction of the pollution scenario.

The prevailing picture is that, in order to match observations, pollution from a primordial generation must be present in the cluster to provide an enriched environment from which a second population forms. Furthermore, extra mixing must be operating in each generation (Suntzeff & Smith 1991; Denissenkov et al. 1998; Briley et al. 1999; Smith 2002) as they ascend the RGB. This is exactly what Smith (2002) suggested is happening in M3. Angelou et al. (2011) provided further evidence for this hypothesis and inferred that the cluster is comprised of two populations[5] with different ages and abundances. It was found that thermohaline mixing can account for the variation in carbon abundance of both the CN-weak and CN-strong stars but only for the nitrogen abundance of the CN-weak stars. The CN-strong stars have so much nitrogen to begin with that any extra mixing does not significantly affect the surface composition. Furthermore, the spread in [N/Fe] is dominated by the variation that was present among the cluster stars before they commenced RGB evolution.

[5] This is not a bold inference. It is expected that almost all GCs contain multiple populations. However, this fact has not been *observationally* confirmed below the RGB of M3.

In this work, we examine the hybrid picture for the chemical evolution of GC giants across a range of metallicity. We investigate the variation of surface [C/Fe] with magnitude on the giant branch of various clusters. The initial abundances are chosen to match the observed subgiant values. We concentrate on C and N because only for these species do data exist over a wide range of luminosities for clusters of different metallicity (data for Li as a function of magnitude exist for M4 and NGC 6397, but the lithium values saturate over a range <1 mag whereas the [C/Fe] show variation over >2 mag; see Mucciarelli et al. 2011 and Lind et al. 2009. Also, measurements of lithium above the LF bump are scarce and many are upper limits rather than detections.). In the intermediate-metallicity clusters we compare M3 to M13. We also turn to the metal-poor regime where Angelou et al. (2010) alluded to significant problems with the contribution of extra mixing in M92; namely, the stars appear to begin mixing before they reach the LF bump. Here we examine a further two similarly metal-poor clusters in M15 and NGC 5466 in order to help identify whether the behavior is due to a unique mixing history in M92 or is common among metal-poor systems.

2. CALCULATIONS

We use MONSTAR (the Monash version of the Mt. Stromlo evolution code; see Campbell & Lattanzio 2008) to produce stellar models for the clusters. Our implementation of thermohaline mixing follows that of Angelou et al. (2011), Charbonnel & Lagarde (2010), Stancliffe (2010), Stancliffe et al. (2009), and Charbonnel & Zahn (2007a, 2007b) in that we use the formulation developed by Ulrich (1972) and Kippenhahn et al. (1980), where thermohaline mixing is modeled as a diffusive process with the coefficient:

$$D_t = C_t\, K \left(\frac{\varphi}{\delta}\right) \frac{-\nabla_\mu}{(\nabla_{\rm ad} - \nabla)} \quad \text{for } \nabla_\mu < 0, \tag{1}$$

where $\varphi = (\partial \ln \rho / \partial \ln \mu)_{P,T}$, $\delta = -(\partial \ln \rho / \partial \ln T)_{P,\mu}$, $\nabla_\mu = (\partial \ln \mu / \partial \ln P)$, $\nabla_{\rm ad} = (\partial \ln T / \partial \ln P)_{\rm ad}$, $\nabla = (\partial \ln T / \partial \ln P)$, K is the thermal diffusivity, and C_t is a dimensionless free parameter. In fact, C_t is related to the aspect ratio, α, of the thermohaline fingers (assumed to be cylindrical) by

$$C_t = \frac{8}{3}\pi^2\alpha^2. \tag{2}$$

Following Angelou et al. (2011), we employ the empirically derived value of $C_t = 1000$ for the stars in GCs. It should be noted that Cantiello & Langer (2010) and Denissenkov (2010) prefer a lower value of $C_t = 12$. Their choice of parameter is based on theoretical grounds and matches the choice of Kippenhahn et al. (1980). Numerical simulations from Denissenkov & Merryfield (2011) and Traxler et al. (2011) also indicate that a value of $C_t = 12$ should be adopted. This value is unable to reproduce observations (Charbonnel & Zahn 2007a; Angelou et al. 2011) but must serve as a caveat to the approach taken in this work. We return to this point in Section 3.3.

2.1. Intermediate Metallicity: M3 and M13

Angelou et al. (2011) showed that the chemical evolution of the stars in M3 is consistent with the hybrid theory of GC evolution. In intermediate-metallicity clusters the contribution of primordial enrichment can be traced through measurements of the CN bands and these were used in M3 to infer the distinct populations. Furthermore, in each population the evolution of [C/Fe] along the RGB was well modeled by thermohaline mixing. It is important to test whether this result pertains to other clusters of similar metallicity. As such we turn our attention to M13. M3 and M13 are a second parameter pair of metallicity [Fe/H] ≈ -1.4 and ages between 11.3 and 14.2 Gyr (Chaboyer et al. 1992; Jimenez et al. 1996; VandenBerg 2000; Salaris & Weiss 2002; Alves et al. 2004). Similarities between the two clusters exist in age, metallicity, Na–O anticorrelation (Sneden et al. 1992; Kraft et al. 1992), Na spread (Cohen 1978; Peterson 1980; Kraft et al. 1992), and *r*-process variation (Roederer 2011); it is only horizontal branch morphology that differs significantly. We therefore expect thermohaline mixing operating in multiple populations to also model the variation of [C/Fe] (and [N/Fe]) in M13.

We use data for M3 and M13 from a variety of sources. The M3 data are taken from Smith (2002), which are compiled from previous studies in the literature, namely Suntzeff (1981), Smith et al. (1996), and Lee (1999) with a zero-point offset applied in order to homogenize the data. In addition to determining carbon and nitrogen abundances as a function of absolute magnitude, Suntzeff (1981) and Norris & Smith (1984) measured the CN strength for M3 giants. We do not possess measurements of CN strength for the stars in the M13 sample, but (unlike M3) observations of [C/Fe] and [N/Fe] exist on the main sequence. For M13 we incorporate the studies of Suntzeff (1981), Smith et al. (1996, 2005), and Briley et al. (2002, 2004). Offsets to allow for systematic differences have been applied by Briley et al. (2004) for all but the most recent study. We assumed a distance modulus of $m - M = 14.43$ which is an average of various measurements ($m - M = 14.44$ from Buckley & Longmore 1992, $m - M = 14.33$ from Harris 1996, $m - M = 14.47$ from Gratton et al. 1997, and $m - M = 14.48$ from Reid 1997). The uncertainty introduced here is no larger than the measurement error of the observations.

In Figure 1, we plot the determined [C/Fe] and [N/Fe] values against absolute visual magnitude for M13 and M3. Symbols are used to specify to which study the data correspond; the legend can be found in the figure. We include two calculations (the two solid curves) used to model M3 (see Angelou et al. 2011). The models are of mass $M = 0.8\,M_\odot$ and metallicity $Z = 0.0005$. In these calculations we run without convective overshoot, our mixing length parameter α is set to 1.75 and thermohaline mixing parameter $C_t = 1000$. In both clusters the solid black curve represents our CN-weak model with initial abundances $Y = 0.2495$, $X(\mathrm{C}) = 5.45 \times 10^{-5}$, $X(\mathrm{N}) = 1.5 \times 10^{-5}$, and $X(\mathrm{O}) = 2.86 \times 10^{-4}$. The initial carbon and nitrogen values were selected to match the measurements of these species in the CN-weak stars in M3. The solid gray curve corresponds to our CN-strong model with $X(\mathrm{C}) = 1.9 \times 10^{-5}$, $X(\mathrm{N}) = 5.5 \times 10^{-5}$, and $X(\mathrm{O}) = 2.6 \times 10^{-4}$ to match the CN-strong population in M3. As the stars are likely to have undergone CN cycling, we increased our ^{4}He to $Y = 0.28$, which only has a marginal effect on the location of the LF bump.

Thermohaline mixing operating in two populations models the behavior of [C/Fe] along the RGB in both M3 and M13. In the case of M13 we have the added constraint of observations along the main sequence. In this cluster, the CN-strong model acts as a lower envelope to the RGB observations and simultaneously accounts for most of the main-sequence data. However, there are a number of subgiant and main-sequence stars at lower [C/Fe] than seen in the M3 data. In order to match the entire main-sequence spread we have taken our

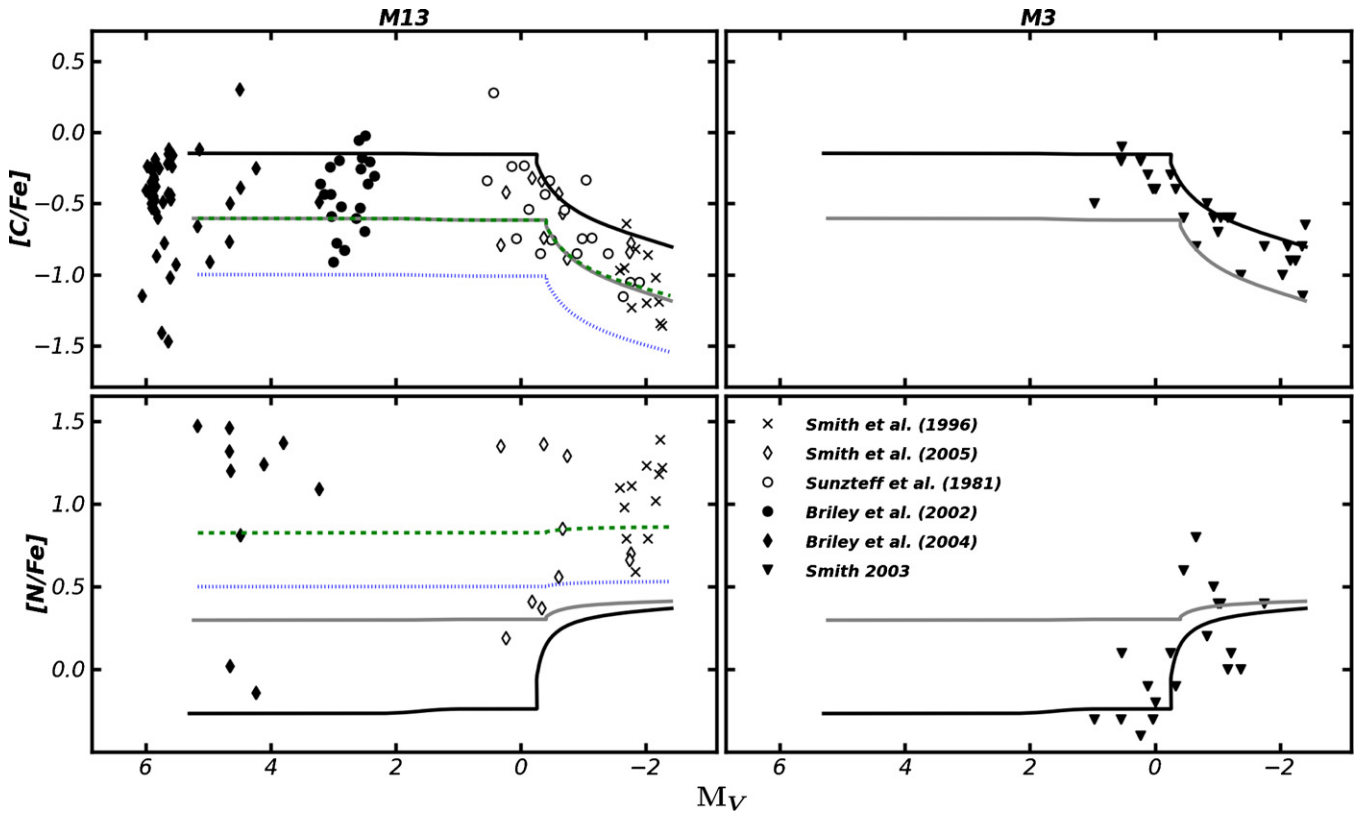

Figure 1. [C/Fe] and [N/Fe] vs. M_V for M13 (left panels) and M3 (right panels). The various studies from which the data are taken are listed in the figure. In all panels the solid black curve represents our CN-weak model and the solid gray curve corresponds to our CN-strong model. For M13 we also provide a nitrogen-enhanced model (green dashed line) and a model designed to match the main-sequence carbon spread of the cluster (blue dotted line). In all models the metallicity is set to $Z = 0.0005$ and the thermohaline mixing parameter $C_t = 1000$.

(A color version of this figure is available in the online journal.)

CN-strong model and reduced the initial carbon by a further 0.4 dex. This is our dotted blue curve where we set initial abundances to $X(\mathrm{C}) = 7.7 \times 10^{-6}$, $X(\mathrm{N}) = 8.8 \times 10^{-5}$, and $X(\mathrm{O}) = 2.4 \times 10^{-4}$. By design this model matches the most carbon-depleted subgiants (except for the three extreme cases with [C/Fe] < -1) but the predicted abundances along the RGB are systematically lower than the current observations. It appears as if these most carbon-depleted subgiants lack counterparts on the RGB. This could be the role of small statistics or the effect of systematic offsets from different data sources; recall that we do not apply an offset for the Smith et al. (2005) study. We are unable to account for the two most carbon-poor stars in M13 ([C/Fe] ≈ -1.5). These stars are at the faint end of the Briley et al. (2004) catalog and hence have large associated errors (J. G. Cohen 2011, private communication).

Compared to M3, there appears to be a larger star-to-star variation in nitrogen in M13; a significantly N-enhanced model is required to reproduce the upper envelope of the data. In the context of the current paradigm, the enrichment is proposed to be due to ON cycling in the polluting generation of stars. To investigate this we constructed an ON-cycled model (dashed green line) with half the oxygen converted to N, giving $X(\mathrm{C}) = 1.9 \times 10^{-5}$, $X(\mathrm{N}) = 1.85 \times 10^{-4}$, and $X(\mathrm{O}) = 1.3 \times 10^{-4}$. The figure shows that the change in [N/Fe] produced by thermohaline mixing is negligible. The initial nitrogen in these stars is sufficiently high that any nitrogen brought to the surface via thermohaline mixing makes little difference to the envelope composition.

We note from Figure 1 that even the ON-cycled model (green dashed line) fails to account for the N-rich stars which show 1 dex more N than this model. Even processing all the O into N would not produce a sufficiently high N abundance. We must consider the possibility, therefore, that C+N+O is higher in M13 than in M3. This is a testable prediction.

As we have stated there are a larger number of stars in M13 that are enriched in nitrogen; Smolinski et al. (2011) find that the cluster contains four times as many CN-strong stars than CN-weak ones. In terms of the hybrid theory, this is interpreted as the cluster containing a majority of second generation stars. In Smith (2002) and Smolinski et al. (2011), the observations suggest that the M3 stars are evenly split among the CN-weak and CN-strong populations. The inferred ratios of the stellar populations within the clusters, determined from measurements of the CN bands, agree with the theoretical predictions of D'Antona & Caloi (2008). They have independently determined that more than 70% of stars in M13 and 50% in M3 are required to be enriched in ^{4}He (a product of CN cycling along with N enrichment) to reproduce the respective horizontal branch morphologies.

In M3, there is a distinct lack of CN-strong stars at low luminosity. As discussed in Angelou et al. (2011), this is an artifact of the original Suntzeff (1981) study in which the lower luminosity stars that were observed happened to be CN weak. Norris & Smith (1984) showed that CN-strong giants do exist in M3 at luminosities corresponding to the faint limit of the Suntzeff (1981) survey, as did Smolinski et al. (2011). The latter show that the CN band strength remains clearly dichotomous in M3 even at low luminosity. We assume this will be reflected in the [N/Fe] abundances and therefore [C/Fe]. So, while we possess measurements of the CN bands for our M3 sample and

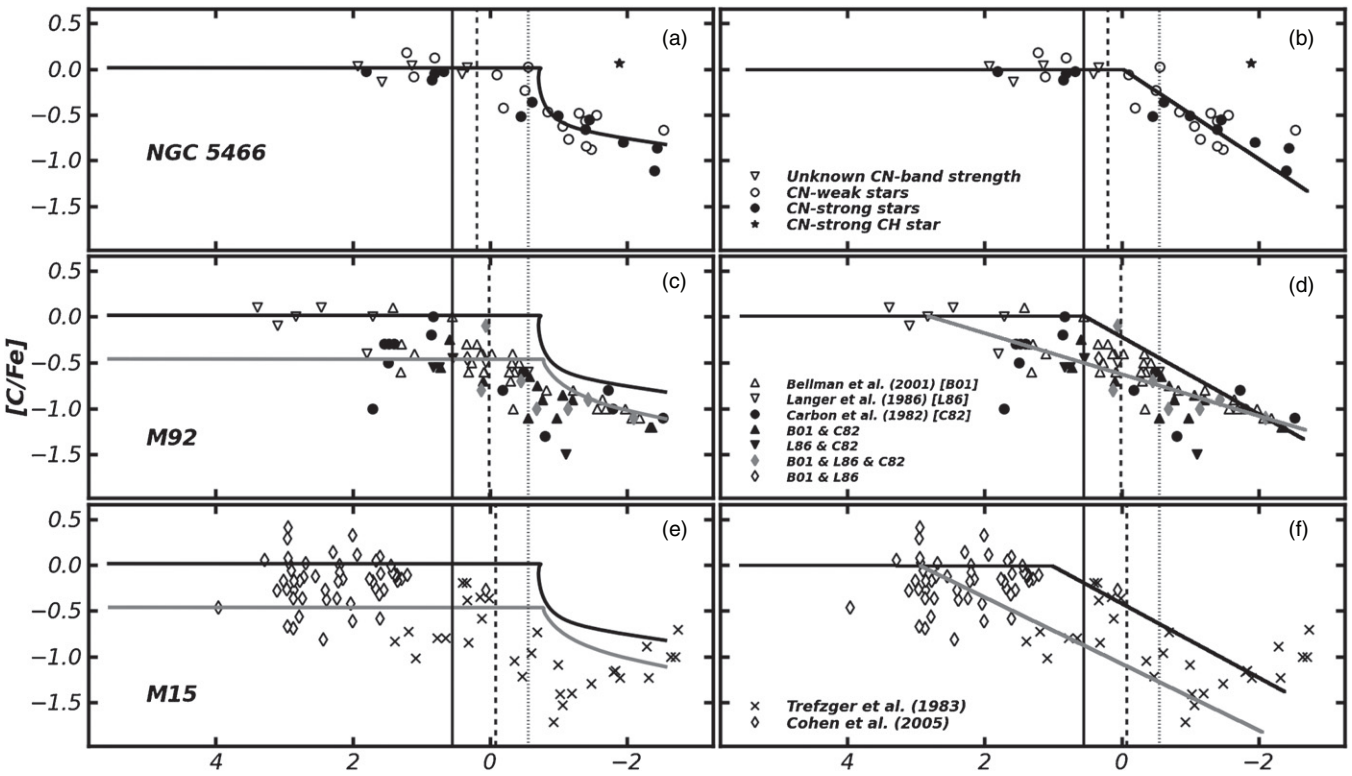

Figure 2. [C/Fe] vs. M_V for NGC 5466 (top panels), M92 (middle panels), and M15 (bottom panels). In the left panels the black curve represents our solar scaled model (CN weak) and the gray curve is our CN-strong model for these clusters. The solid vertical line represents the end of first dredge-up according to the models. The dotted line corresponds to the LF bump according to Martell et al. (2008b). The dashed lines are photometric derivations of the LF bump for each cluster: for M92 and M15 the magnitude is taken from Nataf et al. (2011), and for NGC 5466 from Fekadu et al. (2007). In the right panels we provide lines of best fit by eye, which helps highlight the strange behavior of the clusters.

a few observations of [C/Fe] at low luminosity, conversely in M13 we possess many low-luminosity observations of [C/Fe] but no measurements of the CN bands. Once again the work of Smolinski et al. (2011) provides some insight. They demonstrate an obvious dichotomy in the CN bands along the RGB of M13. The dichotomy is not as clear below the subgiant branch as the temperatures are too high to allow molecule formation. Smolinski et al. (2011) also show a greater spread in the CN band values especially in the CN-strong stars; this is reflected in the large spread in [N/Fe] observed in the cluster.

2.2. Low Metallicity

2.2.1. NGC 5466

Carbon depletion along the RGB of NGC 5466 has been observed by Buonanno et al. (1985), Fekadu et al. (2007), and Shetrone et al. (2010). In this study we use the data from Shetrone et al. (2010); as the observations are from a single instrument, they cover a large luminosity range and for each star [C/Fe] and the CN band strength were determined. As was the case for the intermediate-metallicity clusters, we plot [C/Fe] as a function of absolute visual magnitude. In Figures 2(a) and (b) the NGC 5466 data are plotted according to CN band strength; open circles denote CN-weak stars, and filled circles denote CN-strong stars[6] while triangles represent stars where the CN band strength is unknown. The black solid curve in Figure 2(a) is our thermohaline mixing model with initial abundances of $Y = 0.25$, $X(\mathrm{C}) = 1.6 \times 10^{-5}$, $X(\mathrm{N}) = 5.03 \times 10^{-6}$, and $X(\mathrm{O}) = 4.57 \times 10^{-5}$. The model is of mass $M = 0.8\,M_{\odot}$ and metallicity $Z = 0.0001$ corresponding to the observed [Fe/H] $= -2.2$ and age between 11 and 16 Gyr (di Cecco et al. 2010; Grundahl et al. 2000). We run without convective overshoot, set the mixing length parameter to $\alpha = 1.75$, and set the thermohaline mixing parameter to $C_t = 1000$. Highlighted also are the locations of the important mixing events along the RGB. Common to all panels are the solid vertical line and dotted line. The solid vertical line represents the end of FDU as calculated in the models; this occurs at $M_V \approx 0.56$. The dotted line corresponds to the LF bump at [Fe/H] $= -2.2$, according to Martell et al. (2008b) based on a metallicity–LF-bump relation; this occurs at $M_V \approx -0.55$. For each individual cluster we also include the dashed line which represents a photometrically derived value of the LF bump magnitude. In NGC 5466 this was determined by Fekadu et al. (2007) and occurs at $M_V \approx 0.2 (V_{\mathrm{bump}} = 16.2, (m - M)V = 16.0)$. The end of FDU marks the end of any surface composition changes expected by canonical theory. For stars of this mass and metallicity there is no visible change to the envelope composition from FDU: the change in surface mass fraction of carbon is 6×10^{-8} in our models. The position of the LF bump represents the earliest point at which thermohaline mixing can begin to operate. It corresponds to the point when the hydrogen burning shell meets the composition discontinuity left behind by FDU.

Figure 2(a) suggests that our solar scaled model (black curve) is a good fit to observations of [C/Fe] in NGC 5466. Surface depletion in the cluster appears to begin after the LF bumps determined by Fusi Pecci et al. (1990) and Martell et al. (2008b). We find that the bump determined by Martell et al. (2008b)

[6] The solid star is CN strong but it is most likely a CH star and hence a binary.

is a more convincing fit to the models than that of Fekadu et al. (2007). Fekadu et al. (2007) also inferred the LF bump magnitude by isochrone fitting and obtained a value 0.3 mag brighter. The determination of the LF bump at low metallicity is difficult. We return to this point in Section 3.1

Although a single CN population undergoing thermohaline mixing is a satisfactory fit to the data, in Figure 2(b) we provide an equally plausible fit drawn by eye. The black solid line (which applies to Figures 2(b), (d), and (f)) tries to take into account our belief that carbon depletion should not occur until after FDU but does not take into consideration any preconceptions of the mixing profile. If we assume that the bump luminosity calculated by Fekadu et al. (2007) is correct then depletion begins after the LF bump, as expected. If, however, we use the bump luminosity calculated by Martell et al. (2008b) then the mixing may be argued to begin before the bump is reached.

NGC 5466 requires almost no spread in the initial composition to account for the spread of carbon. In addition to measurements of [C/Fe], Shetrone et al. (2010) analyzed the CN bands of the stars in their sample. The results hinted that a CN dichotomy, which is typical in GC red giants, may be present but as we can see from Figure 2(a) the stars do not separate as clearly as those in the more metal-rich clusters. Shetrone et al. (2010) used a linear least-squares fit in the plane of the S(3839) CN index (Norris et al. 1981) versus absolute V magnitude to divide relatively CN-strong stars (those above the line) from CN-weak stars (those below the line). As in other studies of low-metallicity GCs (e.g., Martell et al. 2008a), the mean separation in CN band strength between the two groups is not large relative to the scatter within each group. While the data suggest that there is a CN bimodality in NGC 5466, its low metallicity reduces the effectiveness of CN band strength as a marker of multiple populations in this cluster.

2.2.2. M92

The M92 data in Figures 2(c) and (d) are those adopted by Smith & Martell (2003) and comprise data from various sources to which offsets have been applied in order to remove systematic differences in abundance scales. These original sources are studies by Carbon et al. (1982), Langer et al. (1986), and Bellman et al. (2001) and we highlight the target stars in each catalog (see the legend in the figure). Even with typical errors of ± 0.2 dex there is a much larger spread in [C/Fe] at any given magnitude than was seen in NGC 5466. In these M92 panels the dotted line is the photometrically derived LF bump identified by Nataf et al. (2011). These authors have utilized high-resolution *Hubble Space Telescope* (*HST*) observations to determine the LF bump in many GCs (see references therein). Their measured value of the magnitude of the bump $M_V \approx 0.016$ ($V_{\rm bump} = 14.666 \pm 0.013$, $(m - M)V = 14.65$) differs from the older Fusi Pecci et al. (1990) value of $M_V \approx -0.39$. We do not possess measurements of CN band strength for the M92 stars plotted in Figures 2(c) and (d) but Norris & Pilachowski (1985) and Smolinski et al. (2011) have provided evidence that a bimodality may exist. As is the case for NGC 5466 the separation in the populations is marginal, a property that appears common at low metallicity. Even without the CN bands the spread in [Na/Fe] (Sneden et al. 1997, 2000), and the spread in [C/Fe] at low luminosities, is evidence for mixing between the two populations.

The depletion of [C/Fe] in M92 has previously been investigated by Denissenkov & VandenBerg (2003) but over a smaller luminosity range. Their (canonical) extra-mixing formulation requires two models, one depleted by 0.1 dex and the other by 0.5 dex in [C/Fe] to match the abundance spread. Angelou et al. (2010) considered the depletion of [C/Fe] with a different implementation of thermohaline mixing to that used here. They highlighted that M92 appeared to show surface depletion of carbon before FDU, a property in disagreement with not just thermohaline mixing but also canonical stellar theory. This strange behavior has been discussed by (at least) Martell et al. (2008b), Gratton et al. (2004), Bellman et al. (2001), and Langer et al. (1986).

This apparent pre-FDU depletion is highlighted in Figure 2(d). Here the black solid line is fit by eye based on the assumption that carbon depletion should not occur until after FDU while the gray curve is a best fit by eye to the data without any preconceived luminosity for the onset of carbon depletion. If we follow the latter fit, then by the time the end of FDU is reached the stars have depleted almost 0.5 dex in [C/Fe]. This is unusual because, as we have stated, at this mass and metallicity we expect changes due to FDU to be of the order of $\Delta X_{\rm Surface}({\rm C}) = 6 \times 10^{-8}$. Between the end of FDU ($M_V \approx +0.5$) and the determined location of the LF bump according to Martell et al. (2008b) ($M_V \approx -0.5$; the earliest point at which thermohaline mixing is expected to begin) the stars in M92 are depleted by roughly a further 0.3 dex in [C/Fe]. Depletion is present but not as pronounced if the Nataf et al. (2011) bump magnitude is used. It is possible that these are the observable effects of other extra-mixing mechanisms and this may also explain the carbon depletion prior to the end of FDU. If true, this would have significant implications for stellar theory. First of all such depletion was not seen in other clusters (Smith & Martell 2003; Shetrone et al. 2010). In most scenarios, extra mixing is inhibited until the star reaches the LF bump and the advancing H-shell removes the molecular weight discontinuity left behind by the receding convective envelope. In the case of M92 some stars on the giant branch have already depleted their [C/Fe] by about 0.8 dex when the models reach this stage. If we have to postulate that some form of mixing begins sufficiently early to produce this depletion, then the mixing must necessarily remove the abundance discontinuity that is itself responsible for the LF bump. If the apparent behavior is real, we believe this is a significant problem for stellar astrophysics.

If we assume that M92 displays an initial spread of [C/Fe] = 0.5 dex then can we remove the issue of mixing before the end of FDU? The black curve in Figure 2(c) is the same solar scaled model applied to match the stars in NGC 5466. As we now require a greater spread in carbon to match this cluster we include a second model (gray solid curve) run with the same physical parameters but a composition that is reduced in C and enhanced in N. For this model we set $Y = 0.25$, $X({\rm C}) = 5.46 \times 10^{-6}$, $X({\rm N}) = 1.60 \times 10^{-5}$, and $X({\rm O}) = 4.57 \times 10^{-5}$, giving [C/Fe] = −0.5. We have not changed Y in the model. The main effect of changing Y is to alter the location of the LF bump, and as we have seen in M3 and M13 this is negligible. These two thermohaline models with large initial carbon spread remove the apparent pre-FDU depletion. Assuming such a spread in [C/Fe] raises the issue that there are no stars observed with [C/Fe] = −0.5 below a magnitude of $M_V \approx 2$. Only four stars have been observed at such magnitudes and all have [C/Fe] ≈ 0. A large spread in [C/Fe] is observed in M15 and M13 below the subgiant branch. We expect this is the case in M92 but require a targeted study to confirm this assumption.

A large spread in [C/Fe] does not solve all the problems associated with M92. Mixing still appears to be occurring before the LF bump, even for the model with an initial [C/Fe] $= -0.5$. There is approximately 1 mag between the locations where the carbon abundances turn down and where the models suggest depletion should begin. Of greater concern is the inability of the models to match the upper RGB abundances of stars in M92. The initial abundances were selected to cover the spread in [C/Fe] before the onset of extra mixing. No stars that have depleted [C/Fe] (magnitude brighter than $M_V = 0$) fall along the evolutionary path predicted by the solar scaled model (black curve). If such stars do exist and are governed by thermohaline mixing, we expect them to be bright members in the cluster (ascending the RGB). It would be perverse if by chance they were not selected for any of the three high-resolution spectrographic studies (unless, of course, they are all in the center of the cluster). The initially depleted model (gray curve) provides an upper envelope to the mixed RGB data; however, the composition was selected to form a lower limit of the initial M92 abundance spread. It is sobering to see how many data points fall below this curve. Although the two models with an initial spread of 0.5 dex in [C/Fe] can encompass fainter stars ($M_V > 0.5$), there are very few stars between the curves once carbon depletion has begun. Thermohaline does not deplete carbon to the levels seen in M92: the models are unable to simultaneously account for both the subgiant branch and RGB data.

The M92 sample is a combination of three different studies and although attempts have been made to homogenize the data, systematic differences in the studies still may lead to offsets of $\simeq$0.3 dex in the [C/Fe] abundances. At such low metallicity one has to wonder if inhomogeneity in the data may be affecting our interpretation of the mixing history. Extensive measurements of [C/Fe] at various magnitudes in this cluster would provide a robust test for stellar evolution models.

2.2.3. M15

[C/Fe] as a function of magnitude is plotted for M15 in Figures 2(e) and (f). The data are a combination of those from Trefzger et al. (1983; crosses) and Cohen et al. (2005; diamonds) and plotted as given in these sources. No offsets have been applied to correct for systematic errors so the data are marked according to their source. As is the case with M92 we do not possess CN band strength measurements for our sample but Smolinski et al. (2011) show there would be little separation between the mean values of the CN-strong and CN-weak stars, a common aspect of the three metal-poor clusters studied here. The same is also true for (at least) NGC 5053, a cluster with metallicity [Fe/H] $= -2.3$ (Smolinski et al. 2011). In Figures 2(e) and (f) the dotted vertical line represents the magnitude of the M15 LF bump determined by Nataf et al. (2011) which occurs at $M_V \approx -0.075$ ($V_{\rm bump} = 15.315 \pm 0.021$, $(m-M)V = 15.39$). This is similar to Zoccali et al. (1999) who also used *HST* data to determine a bump magnitude of $M_V = 0.02 (V_{\rm bump} = 15.41, (m - M)V = 15.39)$.

In Figure 2(e), we plot the two thermohaline mixing models applied in M92. In both clusters thermohaline mixing does not deplete carbon to the degree seen in the observations. Like M92 there is evidence that M15 is mixing between the end of FDU and the LF bump. This is highlighted by Figure 2(f) where we plot our lines drawn by eye rather than the stellar models. This effect would be similar had we adopted the location of the LF bump according to Zoccali et al. (1999). It is possible this is an artifact of combining inhomogeneous data. There is some luminosity overlap between the two studies and it is only when they are combined that it appears as if pre-bump depletion is occurring. This same argument can be used to explain any pre-FDU mixing alluded to by the gray line of best fit in Figure 2(c). A homogeneous set of observations over this luminosity range (as exists for NGC 5466) is required.

While similarities exist there are also slight differences between M15 and M92. A large spread of [C/Fe] is present in M15, which extends below the subgiant branch. This is justification for the inclusion of our initial [C/Fe] $= -0.5$ model (gray curve in Figures 2(c) and (e)). In M92 it is the dearth of observations at low luminosity that raises many questions about the behavior of the cluster and its initial abundance spread. We note there seems to be a lack of stars with high [C/Fe] just before FDU in M15. We assume these stars exist and the current void is a result of combining two studies that focus on stars at different stages of evolution. Perhaps the most curious aspect of M15 is the behavior of the stars at $M_V \approx -1$. The stars appear to suddenly increase their carbon abundance. We await confirmation of this behavior before speculating on its cause as it is inconsistent with our current understanding of stellar nucleosynthesis.

Lind et al. (2009) and Mucciarelli et al. (2011) use lithium to trace extra mixing along the giant branches of NGC 6397 and M4, respectively. Such studies provide a complimentary diagnostic to the variation of C and N with luminosity. Lithium is very sensitive to nuclear burning: it is destroyed at low temperatures. Any transport of material into warmer regions will be reflected through a depletion in the surface lithium abundance. In the case of M15 and M92, this would hopefully help identify the magnitude at which extra mixing begins in these clusters. Given the behavior of M15 and M92 the point at which surface depletion begins (after FDU) must be considered distinct from the LF bump (even though there are good theoretical reasons why the two should coincide as they seem to at higher metallicity). For our purposes we can only rely on high-level photometry (and statistical analysis) of the clusters to distinguish the location of the bump and, as we discuss in Section 3.1, this can be difficult.

3. DISCUSSION

3.1. Comparison across Metallicity

In our two intermediate-metallicity clusters the spread in [C/Fe] is explained by distinct populations which clearly separate according to CN band strength. This is not the case in low-metallicity clusters (Shetrone et al. 2010; Smolinski et al. 2011). Any CN bimodality is marginal at best. The difference between the mean value of a CN index such as S(3839) between CN-strong and CN-weak stars is so small that their distribution can be interpreted as a single CN population with scatter. There is still clear evidence for multiple populations in the metal-poor clusters from the large spreads in O, Na, and Al abundances within them. We therefore expect that a polluting generation will enrich the cluster with CN-processed material and ^{4}He. This should be reflected in the carbon and nitrogen abundances. In M15 there is a large spread in both [C/Fe] ($\approx$1.5 dex) and [N/Fe] ($\approx$3 dex; Cohen et al. 2005) but only a marginal change in the CN bands (Smolinski et al. 2011). In these low-metallicity clusters the CN band strength is not necessarily representative of the nitrogen abundance in the stars.

According to our stellar models with thermohaline mixing, the clusters studied here are close enough in metallicity that we should expect a similar degree of carbon depletion. In the intermediate-metallicity clusters (M3 and M13), we are able to match the depletion of [C/Fe] along the RGB using two models of different initial abundances. In the metal-poor systems thermohaline mixing can account only for the evolution of [C/Fe] in NGC 5466. In M15 and M92 not only do the clusters appear to have depleted far more carbon than we predict but this depletion has begun before the LF bump. Such behavior is not only inconsistent with thermohaline mixing but also standard stellar evolution.

It is worth noting that the LF bump in extremely metal-poor clusters (e.g., M92, M15 and NGC 5466) is not as clearly visible as it is in more metal-rich clusters. There are two theoretical reasons why this is so. First, the depth of FDU is a function of metallicity. Metal-rich stars have deeper convective envelopes than metal-poor stars and therefore a greater discontinuity in the hydrogen profile that develops after FDU. The burning shell in metal-poor stars will encounter a smaller hydrogen difference and spend less time readjusting the stellar structure. Because less time is spent at the magnitude of the bump, the likelihood of observing stars at this location is reduced. Second, evolution on the RGB speeds up as stars move toward brighter luminosities, so the expected number of stars scales inversely with the luminosity in a volume-limited sample (but not in a magnitude-limited sample). Hence the higher the luminosity at which the bump occurs (i.e., the lower the metallicity), the lower the overall number of stars one should expect to observe and the harder it is to identify the bump.

Fusi Pecci et al. (1990) identified an LF bump in M92 by co-adding data for three very similar clusters. Their determined value of $M_V \approx -0.39$ differs slightly from that of Martell et al. (2008b) who find $M_V \approx -0.55$ based on the use of multiple clusters to determine an LF-bump–metallicity relation. Work by Paust et al. (2007) provides little evidence for a bump in the observed LF of M92; however, recent work by Nataf et al. (2011) using *HST* data suggests that it is present at a magnitude of $M_V \approx 0.016$. For NGC 5466, Fekadu et al. (2007) identified a bump using statistical arguments. The bump in M15 was more easily identifiable through the use of *HST* data as was done by Nataf et al. (2011) and Zoccali et al. (1999).

One possible cause for altering the location of the bump (and hence the onset of thermohaline mixing) in our models is to decrease the ^{4}He abundance (Sweigart 1978). However, extrapolating from the Sweigart (1978) results to match the observations would require an initial ^{4}He well below the big bang nucleosynthesis value. Alternatively, if FDU penetrates deeper than the models predict, then the hydrogen burning shell will encounter the homogenized region at lower luminosities. In Figure 3, we plot our metal-poor model with solar scaled abundances in which the convective envelope extended down to a mass of $M = 0.368\,M_\odot$. We have included a model (gray line) with the same initial abundance but artificially homogenized (mixed from the surface) down to a mass of $M = 0.320\,M_\odot$ at the time of FDU. The results show that extending the depth of FDU by about 15% in mass translates to the mixing beginning about 1 mag fainter. Note that the artificial model undergoes a period of adjustment as it returns to the structure of the standard metal-poor model. During this brief phase the burning shell is closer to the homogenized region than the structure would dictate if deeper dredge-up occurred normally. As a consequence the temperatures are such that ^{3}He is easily destroyed but carbon depletion is still inefficient; this can be seen in Figure 3. Angelou et al. (2011) call this situation a "burning-limited" regime. The material is efficiently transported to the desired regions but the processing is inefficient due to the burning conditions. The artificial model therefore has less ^{3}He to drive the mixing near the tip of the RGB when the conditions are more conducive to carbon depletion, a regime Angelou et al. (2011) call "transport limited." In this scenario, the inefficient transport of material to the burning regions is the limiting factor in the processing. This, however, is a side issue stemming from the artificial model; the important point is that one way for the models to match the observations is to make FDU occur deeper in the low-metallicity stars but only low-metallicity stars in M92 and M15.

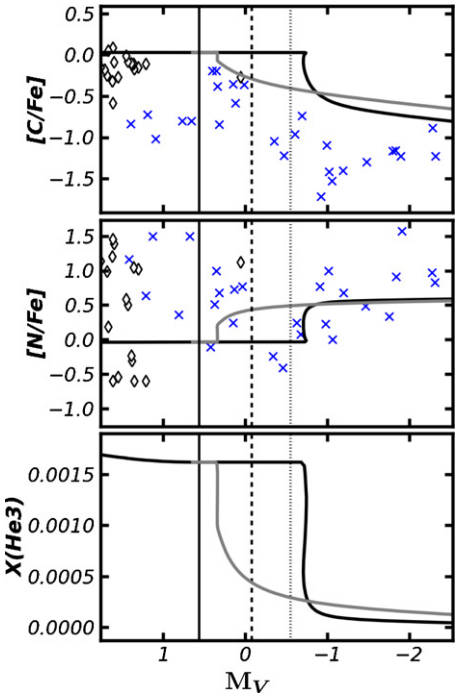

Figure 3. [C/Fe] [N/Fe] and X(^{3}He) vs. M_V for M15. As above the observational data is taken from Trefzger et al. (1983; crosses) and Cohen et al. (2005; diamonds). The solid black curve corresponds to the thermohaline mixing model with standard dredge-up depth (see Figure 2) where the envelope extends down to a depth of $M = 0.368\,M_\odot$. The gray curve represents our model where we have artificially homogenized beyond the depth of first dredge-up to a mass of $M = 0.320\,M_\odot$. The solid vertical line represents the end of first dredge-up according to the normal models. The dotted line corresponds to the LF bump of Martell et al. (2008b) based on a metallicity–LF-bump relation. This occurs at $M_V \approx -0.55$. The dashed line is a photometric derivation of the LF bump taken from Nataf et al. (2011) and occurs at $M_V \approx -0.075$.

(A color version of this figure is available in the online journal.)

3.2. The Inconsistency at Low Metallicity

We are left wondering why there is such an inconsistent picture of GCs at low metallicity. M92 and M15 possess large spreads in [C/Fe] while NGC 5466 shows a much narrower distribution. We find that in the cluster where we have uniform observations thermohaline mixing appears to model the depletion of carbon well. We have already discussed the possibility that combining studies in M15 may be affecting our interpretation of the data. Although data for M92 has been homogenized, it is still the amalgamation of three different studies. Compiling data from various sources may lead to systematic errors. Systematic offsets of 0.3 dex in [C/Fe] are possible and could be the cause of the apparent contradiction.

Because we have two clusters at the same metallicity in M92 and M15 displaying similar behavior, one has to wonder how likely it is that systematic offsets conspire in such a way to appear to give the same effect.

We note that the clusters showing the largest discrepancy with standard models are also the most massive. Having measured the integrated V magnitudes of the three metal-poor clusters Gnedin & Ostriker (1997) find that NGC 5466 ($\approx 1.33 \times 10^5\ M_\odot$) is a lower mass system than M92 ($\approx 3.64 \times 10^5\ M_\odot$) and M15 ($\approx 9.84 \times 10^5\ M_\odot$). This raises the question whether there is a correlation between cluster mass and the extent of primordial [C/Fe] spread at low metallicities. The clusters M15 and M92 may have been able to sustain a greater degree of primordial inhomogeneous carbon enrichment than NGC 5466, with a resulting greater dispersion in [C/Fe] at all magnitudes on the main sequence and RGB than in NGC 5466. The greater range in [C/Fe] along the RGB of M15 and M92 can contribute to a greater observational uncertainty in identifying the magnitude at which carbon depletions produced by extra mixing set in. By contrast, a smaller primordial carbon spread in NGC 5466 produces a more tightly defined locus of [C/Fe] versus M_V on the RGB of that cluster, making it a preferable test case for mixing studies. When comparing the r-process elements both M92 and M15 show similar star-to-star variations (Roederer 2011; Roederer & Sneden 2011; although this has recently been questioned by Cohen 2011) which may add additional support to the Na and O abundance evidence that both clusters have sustained heterogeneous enrichment across a range of chemical elements. It would be interesting to determine the O, Na, and r-process element patterns in NGC 5466 to see if they are more homogeneous than in M92 and M15, as a mass-dependent primordial enrichment scenario would anticipate.

3.3. The Role of Thermohaline Mixing

It is of course possible that thermohaline mixing does not govern the surface composition of low-mass giants. It is not the only process by which mixing may occur in the radiative zone. Mechanisms such as those listed in Section 1 may also be involved. The way in which these mechanisms interact is uncertain and as they are inherently three dimensional our understanding of their behavior will improve with the study of these processes in hydrodynamical codes (Dearborn et al. 2001; Bazan et al. 2001; Turcotte et al. 2002; Eggleton et al. 2002; Bazán et al. 2003). Still, the current generation of one-dimensional codes are the precursors to more sophisticated modeling and much insight can be gained through them. One-dimensional spherically symmetric models with multiple extra-mixing mechanisms include those of Cantiello & Langer (2010) and Charbonnel & Lagarde (2010), both of whom demonstrate that the thermohaline mixing diffusion coefficient is larger than the radial component of rotational mixing. The former also show the thermohaline coefficient to be larger than that of magnetic buoyancy. These codes do not explicitly treat the interaction of the mixing mechanisms and how any given instability may react due to the presence of other processes; rather, they simply add the diffusion coefficients. Charbonnel & Zahn (2007b) have investigated an instance of multi-process interaction through linear analysis and argue that magnetic fields could serve to inhibit the effects of thermohaline mixing.

Charbonnel & Lagarde (2010) and Lagarde et al. (2011) have produced detailed rotational-thermohaline mixing models for stars of various mass and metallicity. They find rotation leads to a deeper penetration of the convective envelope than their non-rotating models. This allows rotational models to begin thermohaline mixing at fainter magnitudes than their static models; this may go some way to reconciling the magnitude at which stars in M92 and M15 begin mixing. It should be noted that low-mass, low-metallicity rotational models have been produced by Palacios et al. (2006) and Denissenkov et al. (2006), and in the former the depth of FDU depends on the rotational model used. A window of 0.13 mag is possible for the location of the bump depending on the treatment of rotational physics. That is, different implementations of rotation can move the location of the LF bump to higher or lower magnitudes. Different models of rotational mixing are at play here, in much the same way that different codes produce different third dredge-up results based on the treatment of convective stability (Herwig 2005). However, stochastic variations such as rotation may lead to deeper FDU in the stars of M15 and M92. Peterson (1983) have shown that stars on the horizontal branch of M13 rotate twice as fast as those on the horizontal branch of M3. Although we find no major discrepancies between the location of the LF bump in these two clusters (0.07 mag; Nataf et al. 2011), in the case of M15 and M92 the effect of rotation on the depth of the FDU may be more pronounced. Why the stars in M13 would rotate faster than the stars in M3 would also require an explanation.

While it is generally agreed that the burning of ^{3}He in a homogenized zone causes an instability, the efficiency of the resultant mixing has been the cause for debate. The exact value of C_t to adopt remains contentious. Recent multi-dimensional models of thermohaline mixing by Denissenkov (2010), Denissenkov & Merryfield (2011), and Traxler et al. (2011) support the view of Cantiello & Langer (2010) and the suggestion by Kippenhahn et al. (1980) that the "aspect ratio," α, of the rising element should take a value of $\alpha \approx 1$ ($C_t \approx 12$). Laboratory experiments by Stommel and Faller published in Stern (1960) have lead Ulrich (1972) and Charbonnel & Zahn (2007a) to prefer a value of α somewhere closer to $\alpha \approx 6$ ($C_t \approx 1000$). Indeed there is great empirical evidence to prefer this value as it appears to match observations of stars across a great range of mass and metallicity. The mechanism is an elegant means of matching C and N abundances in various stars as well as ensuring measurements of ^{3}He in H II regions are consistent with predictions from stellar models and big bang nucleosynthesis (Rood et al. 1984; Hogan 1995; Charbonnel 1995; Charbonnel & Do Nascimento 1998; Tosi 1998; Palla et al. 2000; Romano et al. 2003). Canonical models predict that low-mass, main-sequence stars are net producers of ^{3}He, which is returned to the interstellar medium through mass loss. Hata et al. (1995) have shown that about 90% of the ^{3}He produced on the main sequence must be destroyed to reconcile the two fields. Our preferred value of $C_t = 1000$ matches the carbon and nitrogen in clusters and also destroys over 90% of the ^{3}He in the star before the tip of the RGB. The lower value of $C_t = 12$ once again creates a discrepancy between measurements of ^{3}He in H II regions as only ≈20% of the initial ^{3}He is destroyed, meaning low-mass stars are once again producers of ^{3}He.

It is the aim of this work and in Angelou et al. (2011) to rely on empirical evidence to determine the best value of C_t to use in the one-dimensional codes. In the models presented here C_t has been fixed at a value of 1000. This is consistent with previous studies where the same factor has reproduced observations of GC stars (Angelou et al. 2011), field stars (Charbonnel & Lagarde 2010), and where the mixing has been used to explain the dichotomy between extremely metal-poor stars and

carbon-enhanced metal-poor stars (Stancliffe et al. 2009; although the latter point is in disagreement with Denissenkov & Pinsonneault 2008a, 2008b). Angelou et al. (2011) demonstrate that once C_t exceeds 1000, the processing enters into the burning-limited regime whereby increasing the diffusion coefficient has little effect on the final surface abundances. They also show that values of $C_t < 600$ simply lead to less mixing than is required to match the observations. Although we are modeling the mixing as *diffusive*, it is in fact an *advective* process. We have implemented a linear model of thermohaline mixing that operates via a diffusion equation. Recent three-dimensional numerical simulations of thermohaline mixing (Denissenkov & Merryfield 2011; Traxler et al. 2011) find blob-like structures, which are identified with the aspect ratio of the idealized "fingers" in the one-dimensional derivation of Ulrich (1972). It is from this identification that the preference for low values of C_t in the numerical simulations is based. Numerical simulations are a very powerful tool, but are subject to numerous caveats—resolution (time and space), viscosity (numerical and molecular), and extrapolation to stellar conditions (e.g., Prandtl numbers that are $\approx 10^5$ too large). In view of these uncertainties, we feel it premature to draw definite conclusions from the numerical simulations. Nonetheless, if the low values of C_t coming from the simulations prove to hold then it would result in a conclusion that either the diffusive approximation to thermohaline mixing used here is not applicable or that thermohaline mixing is too weak to produce the observed carbon depletions of GC red giants.

4. CONCLUSIONS

We have modeled the depletion of carbon via thermohaline mixing on the RGB of the intermediate-metallicity clusters M3 and M13 as well as the metal-poor clusters NGC 5466, M92, and M15. We conclude the following.

1. Thermohaline mixing in the presence of primordial enrichment can account for the carbon variation seen in M3 and M13. The spread of carbon along the RGB in both clusters can be covered by the same set of models. In order to match the main-sequence spread in M13, we require a model further depleted in [C/Fe]. This model, however, predicts that some stars on the RGB should have [C/Fe] values lower than seen. The majority of stars in M13 are enriched in nitrogen while about half the stars in M3 appear to be CN strong. The results from the hybrid picture here are consistent with the findings of D'Antona & Caloi (2008) and their requirements to match the horizontal branch morphologies of the clusters. In their work the enriched ^{4}He of the second population acts as the second parameter and helps dictate where the star falls along the horizontal branch. The stars in M13 that are most enriched in [N/Fe] suggest they were formed with some primary nitrogen (higher C+N+O than those in M3).
2. Thermohaline mixing can explain carbon depletion with magnitude in NGC 5466. A single solar scaled model is sufficient to explain the cluster even though a modest CN spread has been determined (Shetrone et al. 2010). Our models provide a good fit for this cluster if we adopt the LF bump determined by Martell et al. (2008b). However, the data do not exclude the possibility that NGC 5466 is depleting carbon before the LF bump as seems to be the case for M15 and M92.
3. In M92 and M15 we have combined observations of [C/Fe] from multiple studies. Thermohaline mixing is unable to reproduce the evolution of carbon along the giant branch in these clusters. The models do not deplete carbon rapidly enough along the RGB. In addition, depletion appears to begin before FDU in M92, although this may be due to the fact that we only have a few observations at low luminosity. A targeted study at low luminosity is required to confirm if the cluster has the same spread in [C/Fe] as M15. Both clusters appear to be mixing before the LF bump and bright stars are not observed near the predicted carbon abundances for initial [C/Fe] = 0.
4. Both M92 and M15 seem to require deeper FDU in order for the models to fit the current observations, but this is not the case for NGC 5466.
5. A consideration that inevitably has to serve as a caveat to our discussions is that the comparison between the thermohaline-mixing models and the [C/Fe] as a function of magnitude data may be hindered by the heterogeneity of the latter, particularly in clusters such as M92 and M15 where zero-point offsets of up to 0.3 dex may exist between the various data sources compiled. Although attempts have been made to compensate for these, it remains nonetheless a source of concern. Determining the behavior of carbon to faint luminosities on the RGB in both M92 and M15 as well as M3, using a single spectrograph and data analysis system, could provide a more homogeneous and rigorous test of our models. Such data would need to include C and N values for subgiants also. In addition, observations of lithium abundances over a large luminosity range can be used to better define the character of extra mixing, while measurements of nitrogen, oxygen, and/or sodium abundances can define the patterns of primordial enrichment within the clusters.

We thank Matt Shetrone and Sarah Martell for discussions with us at Nuclei in the Cosmos XI. We also thank Sandro Chieffi and Marco Limongi for comparing their models with us and demonstrating in detail the effects of rotation. We also thank Sandro for discussions on the LF bump in low-luminosity clusters and Judy Cohen for her help with the M13 data. G.C.A. acknowledges the financial support of the APA scholarship. R.P.C. is funded by a Marie-Curie Intra-European fellowship, grant No. 252431, under the European Commission's FP7 framework. R.J.S. is a Stromlo fellow and during his time at Monash, he was funded by the Australian Research Council's Discovery Projects Scheme under grant DP0879472. This work was supported by the NCI National Facility at the ANU.

REFERENCES

Alves, D. R., Cook, K. H., & Wishnow, E. 2004, BAAS, 36, 1425
Anderson, J., Piotto, G., King, I. R., Bedin, L. R., & Guhathakurta, P. 2009, ApJ, 697, L58
Angelou, G. C., Church, R. P., Stancliffe, R. J., Lattanzio, J. C., & Smith, G. H. 2011, ApJ, 728, 79
Angelou, G. C., Lattanzio, J. C., Church, R. P., & Stancliffe, R. J. 2010, Mem. Soc. Astron. Ital., 81, 1057
Arp, H. C. 1955, AJ, 60, 317
Arp, H. C., Baum, W. A., & Sandage, A. R. 1952, AJ, 57, 4
Bazan, G., Castor, J., Dearborn, D. S. P., et al. 2001, BAAS, 31, 1369
Bazán, G., Dearborn, D. S. P., Dossa, D. D., et al. 2003, in ASP Conf. Ser. 293, 3D Stellar Evolution, ed. S. Turcotte, S. C. Keller, & R. M. Cavallo (San Francisco, CA: ASP), 1
Bellman, S., Briley, M. M., Smith, G. H., & Claver, C. F. 2001, PASP, 113, 326
Briley, M. M., & Cohen, J. G. 2001, AJ, 122, 242

Briley, M. M., Cohen, J. G., & Stetson, P. B. 2002, ApJ, 579, L17
Briley, M. M., Cohen, J. G., & Stetson, P. B. 2004, AJ, 127, 1579
Briley, M. M., Grundahl, F., & Andersen, M. I. 1999, BAAS, 31, 1369
Briley, M. M., Hesser, J. E., & Bell, R. A. 1991, ApJ, 373, 482
Brown, J. A., & Wallerstein, G. 1993, AJ, 106, 133
Buckley, D. R. V., & Longmore, A. J. 1992, MNRAS, 257, 731
Buonanno, R., Corsi, C. E., Buzzoni, A., et al. 1994, A&A, 290, 69
Buonanno, R., Corsi, C. E., & Fusi Pecci, F. 1985, A&A, 145, 97
Busso, M., Wasserburg, G. J., Nollett, K. M., & Calandra, A. 2007, ApJ, 671, 802
Campbell, S. W., & Lattanzio, J. C. 2008, A&A, 490, 769
Cannon, R. D., Croke, B. F. W., Bell, R. A., Hesser, J. E., & Stathakis, R. A. 1998, MNRAS, 298, 601
Cantiello, M., & Langer, N. 2010, A&A, 521, A9
Carbon, D. F., Romanishin, W., Langer, G. E., et al. 1982, ApJS, 49, 207
Catelan, M., Borissova, J., Ferraro, F. R., et al. 2002, AJ, 124, 364
Chaboyer, B., Sarajedini, A., & Demarque, P. 1992, ApJ, 394, 515
Chanamé, J., Pinsonneault, M., & Terndrup, D. M. 2005, ApJ, 631, 540
Charbonnel, C. 1995, ApJ, 453, L41
Charbonnel, C. 2010, IAUS, 266, 131
Charbonnel, C., Brown, J. A., & Wallerstein, G. 1998, A&A, 332, 204
Charbonnel, C., & Do Nascimento, J. D., Jr. 1998, A&A, 336, 915
Charbonnel, C., & Lagarde, N. 2010, A&A, 522, A10
Charbonnel, C., & Zahn, J. 2007a, A&A, 467, L15
Charbonnel, C., & Zahn, J. 2007b, A&A, 476, L29
Cohen, J. G. 1978, ApJ, 223, 487
Cohen, J. G. 1999, AJ, 117, 2428
Cohen, J. G. 2011, ApJ, 740, L38
Cohen, J. G., Briley, M. M., & Stetson, P. B. 2005, AJ, 130, 1177
Cohen, J. G., & Meléndez, J. 2005, AJ, 129, 303
D'Antona, F., Bellazzini, M., Caloi, V., et al. 2005, ApJ, 631, 868
D'Antona, F., & Caloi, V. 2008, MNRAS, 390, 693
Dearborn, D. S. P., Bazan, G., Castor, J., et al. 2001, BAAS, 33, 886
Decressin, T., Meynet, G., Charbonnel, C., Prantzos, N., & Ekström, S. 2007, A&A, 464, 1029
de Mink, S. E., Pols, O. R., Langer, N., & Izzard, R. G. 2009, A&A, 507, L1
Denissenkov, P. A. 2010, ApJ, 723, 563
Denissenkov, P. A., Chaboyer, B., & Li, K. 2006, ApJ, 641, 1087
Denissenkov, P. A., Da Costa, G. S., Norris, J. E., & Weiss, A. 1998, A&A, 333, 926
Denissenkov, P. A., & Merryfield, W. J. 2011, ApJ, 727, L8
Denissenkov, P. A., & Pinsonneault, M. 2008a, ApJ, 679, 1541
Denissenkov, P. A., & Pinsonneault, M. 2008b, ApJ, 684, 626
Denissenkov, P. A., Pinsonneault, M., & MacGregor, K. B. 2009, ApJ, 696, 1823
Denissenkov, P. A., & Tout, C. A. 2000, MNRAS, 316, 395
Denissenkov, P. A., & VandenBerg, D. A. 2003, ApJ, 593, 509
di Cecco, A., Becucci, R., Bono, G., et al. 2010, PASP, 122, 991
Eggleton, P. P., Bazan, G., Cavallo, R. M., et al. 2002, BAAS, 35, 570
Eggleton, P. P., Dearborn, D. S. P., & Lattanzio, J. C. 2006, Science, 314, 1580
Eggleton, P. P., Dearborn, D. S. P., & Lattanzio, J. C. 2008, ApJ, 677, 581
Fekadu, N., Sandquist, E. L., & Bolte, M. 2007, ApJ, 663, 277
Fenner, Y., Campbell, S., Karakas, A. I., Lattanzio, J. C., & Gibson, B. K. 2004, MNRAS, 353, 789
Fusi Pecci, F., Ferraro, F. R., Crocker, D. A., Rood, R. T., & Buonanno, R. 1990, A&A, 238, 95
Gnedin, O. Y., & Ostriker, J. P. 1997, ApJ, 474, 223
Gratton, R., Sneden, C., & Carretta, E. 2004, ARA&A, 42, 385
Gratton, R. G., Fusi Pecci, F., Carretta, E., et al. 1997, ApJ, 491, 749
Gratton, R. G., Sneden, C., Carretta, E., & Bragaglia, A. 2000, A&A, 354, 169
Grundahl, F., VandenBerg, D. A., Bell, R. A., Andersen, M. I., & Stetson, P. B. 2000, AJ, 120, 1884
Harris, W. E. 1996, AJ, 112, 1487
Hata, N., Scherrer, R. J., Steigman, G., et al. 1995, Phys. Rev. Lett., 75, 3977
Herwig, F. 2005, ARA&A, 43, 435
Hesser, J. E., & Bell, R. A. 1980, ApJ, 238, L149
Hogan, C. J. 1995, ApJ, 441, L17
Hubbard, E. N., & Dearborn, D. S. P. 1980, ApJ, 239, 248
Iben, I., Jr. 1967, ApJ, 147, 624
Iben, I., Jr., & Ehrman, J. R. 1962, ApJ, 135, 770
Iben, I., Jr., & Faulkner, J. 1968, ApJ, 153, 101
Jimenez, R., Thejll, P., Jorgensen, U. G., MacDonald, J., & Pagel, B. 1996, MNRAS, 282, 926
Johnson, H. L., & Sandage, A. R. 1955, ApJ, 121, 616
Kippenhahn, R., Ruschenplatt, G., & Thomas, H. 1980, A&A, 91, 175
Kraft, R. P. 1994, PASP, 106, 553
Kraft, R. P., Sneden, C., Langer, G. E., & Prosser, C. F. 1992, AJ, 104, 645
Lagarde, N., Charbonnel, C., Decressin, T., & Hagelberg, J. 2011, A&A, 536, A28
Langer, G. E., Kraft, R. P., Carbon, D. F., Friel, E., & Oke, J. B. 1986, PASP, 98, 473
Lee, S. 1999, AJ, 118, 920
Lee, Y., Joo, S.-J., Han, S.-I., et al. 2005, ApJ, 621, L57
Lind, K., Primas, F., Charbonnel, C., Grundahl, F., & Asplund, M. 2009, A&A, 503, 545
Martell, S. L., Smith, G. H., & Briley, M. M. 2008a, PASP, 120, 7
Martell, S. L., Smith, G. H., & Briley, M. M. 2008b, AJ, 136, 2522
Mucciarelli, A., Salaris, M., Lovisi, L., et al. 2011, MNRAS, 412, 81
Nataf, D. M., Gould, A. P., Pinsonneault, M. H., & Udalski, A. 2011, arXiv:1109.2118
Nordhaus, J., Busso, M., Wasserburg, G. J., Blackman, E. G., & Palmerini, S. 2008, ApJ, 684, L29
Norris, J., Cottrell, P. L., Freeman, K. C., & Da Costa, G. S. 1981, ApJ, 244, 205
Norris, J., & Pilachowski, C. A. 1985, ApJ, 299, 295
Norris, J., & Smith, G. H. 1984, ApJ, 287, 255
Oke, J. B., & Schwarzschild, M. 1952, ApJ, 116, 317
Osborn, W. 1971, Observatory, 91, 223
Palacios, A., Charbonnel, C., Talon, S., & Siess, L. 2006, A&A, 453, 261
Palla, F., Bachiller, R., Stanghellini, L., Tosi, M., & Galli, D. 2000, A&A, 355, 69
Palmerini, S., Busso, M., Maiorca, E., & Guandalini, R. 2009, PASA, 26, 161
Palmerini, S., Cristallo, S., Busso, M., et al. 2011a, ApJ, 741, 26
Palmerini, S., La Cognata, M., Cristallo, S., & Busso, M. 2011b, ApJ, 729, 3
Pancino, E., Rejkuba, M., Zoccali, M., & Carrera, R. 2010, A&A, 524, A44
Paust, N. E. Q., Chaboyer, B., & Sarajedini, A. 2007, AJ, 133, 2787
Pavlenko, Y. V., Jones, H. R. A., & Longmore, A. J. 2003, MNRAS, 345, 311
Peterson, R. C. 1980, ApJ, 237, L87
Peterson, R. C. 1983, ApJ, 275, 737
Pilachowski, C., Sneden, C., Freeland, E., & Casperson, J. 2003, AJ, 125, 794
Piotto, G. 2009, IAUS, 258, 233
Piotto, G., Bedin, L. R., Anderson, J., et al. 2007, ApJ, 661, L53
Piotto, G., Villanova, S., Bedin, L. R., et al. 2005, ApJ, 621, 777
Popper, D. M. 1947, ApJ, 105, 204
Recio-Blanco, A., & de Laverny, P. 2007, A&A, 461, L13
Reid, I. N. 1997, AJ, 114, 161
Roederer, I. U. 2011, ApJ, 732, L17
Roederer, I. U., & Sneden, C. 2011, AJ, 142, 22
Romano, D., Tosi, M., Matteucci, F., & Chiappini, C. 2003, MNRAS, 346, 295
Rood, R. T., Bania, T. M., & Wilson, T. L. 1984, ApJ, 280, 629
Salaris, M., & Weiss, A. 2002, A&A, 388, 492
Sandage, A. R. 1953, AJ, 58, 61
Sandage, A. R. 1954, Mem. Soc. R. Sci. Liege, 1, 254
Shetrone, M., Martell, S. L., Wilkerson, R., et al. 2010, AJ, 140, 1119
Shetrone, M. D. 2003, ApJ, 585, L45
Smith, G. H. 2002, PASP, 114, 1097
Smith, G. H. 2006, PASP, 118, 1225
Smith, G. H., Briley, M. M., & Harbeck, D. 2005, AJ, 129, 1589
Smith, G. H., & Martell, S. L. 2003, PASP, 115, 1211
Smith, G. H., Shetrone, M. D., Bell, R. A., Churchill, C. W., & Briley, M. M. 1996, AJ, 112, 1511
Smolinski, J. P., Martell, S. L., Beers, T. C., & Lee, Y. S. 2011, AJ, 142, 1268
Sneden, C., Kraft, R. P., Guhathakurta, P., Peterson, R. C., & Fulbright, J. P. 2004, AJ, 127, 2162
Sneden, C., Kraft, R. P., Prosser, C. F., & Langer, G. E. 1992, AJ, 104, 2121
Sneden, C., Kraft, R. P., Shetrone, M. D., et al. 1997, AJ, 114, 1964
Sneden, C., Pilachowski, C. A., & Kraft, R. P. 2000, AJ, 120, 1351
Sneden, C., Pilachowski, C. A., & Vandenberg, D. A. 1986, ApJ, 311, 826
Sollima, A., Ferraro, F. R., Bellazzini, M., et al. 2007, ApJ, 654, 915
Spite, M., Cayrel, R., Plez, B., et al. 2005, A&A, 430, 655
Spite, M., Cayrel, R., Hill, V., et al. 2006, A&A, 455, 291
Stancliffe, R. J. 2010, MNRAS, 403, 505
Stancliffe, R. J., Church, R. P., Angelou, G. C., & Lattanzio, J. C. 2009, MNRAS, 396, 2313
Stern, M. 1960, Tellus, 12, 172
Suntzeff, N. B. 1981, ApJS, 47, 1
Suntzeff, N. B., & Smith, V. V. 1991, ApJ, 381, 160
Sweigart, A. V. 1978, in IAU Symp. 80, The HR Diagram—The 100th Anniversary of Henry Norris Russell, ed. A. G. D. Philip & D. S. Hayes (Dordrecht: Reidel), 333
Sweigart, A. V., & Mengel, J. G. 1979, ApJ, 229, 624
Tosi, M. 1998, Space Sci. Rev., 84, 207
Traxler, A., Garaud, P., & Stellmach, S. 2011, ApJ, 728, L29

Trefzger, D. V., Langer, G. E., Carbon, D. F., Suntzeff, N. B., & Kraft, R. P. 1983, ApJ, 266, 144
Turcotte, S., Bazan, G., Castor, J., et al. 2002, in ASP Conf. Ser. 259, IAU Colloq. 185: Radial and Nonradial Pulsations as Probes of Stellar Physics, ed. C. Aerts, T. R. Bedding, & J. Christensen-Dalsgaard (San Francisco, CA: ASP), 72
Ulrich, R. K. 1972, ApJ, 172, 165
VandenBerg, D. A. 2000, ApJS, 129, 315
Ventura, P., & D'Antona, F. 2011, MNRAS, 410, 2760
Wachlin, F. C., Miller Bertolami, M. M., & Althaus, L. G. 2011, A&A, 533, A139
Wasserburg, G. J., Boothroyd, A. I., & Sackmann, I. 1995, ApJ, 447, L37
Zoccali, M., Cassisi, S., Piotto, G., Bono, G., & Salaris, M. 1999, ApJ, 518, L49